

## Sintering BFO targets for RF sputtering

G. Orr, A. Goryachev, G. Golan\*

Ariel University, Science Park, Ariel 40700, Israel

Ceramic  $BiFeO_3$  samples were prepared by rapid sintering at  $880^\circ C$ . Two compositions were examined. A 56/44  $Bi_2O_3/Fe_2O_3$  mole% composition and a  $56Bi_2O_3\ 44Fe_2O_3 + 6.5wt\%\ NaCl$  composition. The samples were heat treated at different times up to 8 minutes and the phase content was examined as a function of the time using XRD measurements and analysis. It was demonstrated that using both compositions, maximum  $BiFeO_3$  phase content is obtained after 3.5 minutes. In the former approximately 50% of the material transformed to  $BiFeO_3$  while in the latter 98.5%.

**Keywords:** BFO, sputtering, photovoltaic, multiferroic

### INTRODUCTION

BFO has regained much interest in recent years due to its multiferroic nature [1]. It is one of the few known materials which simultaneously possess both ferroelectric and ferromagnetic ordering at room temperature. It has promising applications in photovoltaics, and due to the magneto-electric coupling between the electric and magnetic polarization providing for new device design. As such, the material shows much promise in realizing spintronic devices, sensors and multistate memory devices [1, 2]. It has been demonstrated [3] that impurities will result in additional phases, the more common and stable ones being the  $Bi_2Fe_4O_9$  (mullite) and  $Bi_{25}FeO_{40}$  (sillenite) with a relatively short lived phase of  $BiFeO_3$  (BFO). Of the two variants ( $BiFeO_3$ ,  $Bi_2Fe_4O_9$ ) much work has been done in sintering ceramics composed of the variety of phases with the aim of obtaining materials which are composed mostly of  $BiFeO_3$  nano crystallites. This is required for fabricating experimental devices based on deposition of thin films such as spintronics based components and sensors.  $BiFeO_3$  sintered ceramic disks may be used as targets for the thin film deposition process. While all three phases appear at different ratios within the sintered material, we can expect that those phases with the greater change in Gibbs energy will be more stable. Based on experimental work, Phapale et al. [4] evaluated the heat capacity and derived the standard Gibbs energy of formation for the above compounds from room temperature up to  $640^\circ C$ . Selbach et. al. expanded this work demonstrating that at the temperature range of  $447\sim 767^\circ C$  Gibbs energy of formation of  $BiFeO_3$  is a metastable compound which would be the first to

nucleate but would eventually transform into  $Bi_2Fe_4O_9$  and  $Bi_{25}FeO_{40}$ . But above  $767^\circ C$  increasing to the proximity of the peritectic temperature at  $930^\circ C$ , or below it is a stable compound. Carvalho et. al. [5] using sol-gel combustion to create ceramic samples of  $BiFeO_3$  have also demonstrated similar results to Selbach's work. They further demonstrate that at a temperature of  $600^\circ C$  the  $BiFeO_3$  transforms into the more stable mullite phase  $Bi_2Fe_4O_9$  over many hours. This is the reasoning behind the short period heating and rapid cooling techniques for obtaining BFO ceramics [6, 7, 8]. Using ultra-pure starting materials Lu et. al. [3] tested the stability as a function of the crucible type (gold or aluminium oxide) and the process from which the compound was synthesized. The processes consisted of solid-state reaction of the starting materials without reducing parasitic phases using  $HNO_3$ , solid state reaction of the materials followed by parasitic phase reduction and crushed crystals. Composition stability was tested at  $850^\circ C$  for 24 and 48 hours and  $855^\circ C$  for 24 hours. Both temperatures are above  $767^\circ C$  so we should expect them to form the more stable  $BiFeO_3$  phase. After 48 hours at  $850^\circ C$  both the phase reduced (alumina crucible) and the crushed crystal (gold crucible) did not decompose, while after 24 hours 44% of the non reduced compound decomposed. At  $855^\circ C$  after 24 hours, 7% of the crushed crystals in gold crucible, 26% of the parasitic phase reduced in gold crucible, and 87% of the parasitic phase reduced in alumina crucible decomposed. Evidently, and as expected at  $850^\circ C$  BFO is the stable phase, at the same temperature the material without parasitic phase reduction decomposed considerably. The important point to consider is that the  $HNO_3$  treatment dissolves every compound but the BFO and the  $Bi_2Fe_4O_9$ , thus without such a treatment, some phase

\* To whom all correspondence should be sent:  
gadygo@ariel.ac.il

impurities and not necessarily only the sillenite phase exist resulting in an increased decomposition. At 855°C the volatility of bismuth comes into play. Lu claims it is a phase transformation, but we doubt it, as no one has observed a phase transformation at that temperature, and that includes the DSC (Differential scanning calorimetry) results that they present in the mentioned article. It is more likely a compositional change due to bismuth evaporation. Considering the parasitic reduced phase in the alumina crucible, something totally different is happening. According to the published phase diagrams [9, 10, 11, 3] we should not expect the mullite phase unless we exceed 930°C or if we suffer from considerable evaporation of bismuth. Hence, we are drawn to suspect that the existence of the mullite phase in areas which it is not a favourable phase is indicative of impurities.

In order to test this assumption, we will compare a  $\text{Bi}_2\text{O}_3$  saturated composition against the same  $\text{Bi}_2\text{O}_3$  saturated composition but with  $\text{NaCl}$  as an impurity.

## EXPERIMENTAL

### Material synthesis and sintering

The starting materials for the samples which were sintered are based on what was found to be the optimal composition by Bush et. al and Gabbasova et. al [12] for growing BFO macroscopic crystals from the melt. Analytical grade chemicals were selected,  $\text{Bi}_2\text{O}_3$  (Merck 99.99% typ.),  $\text{Fe}_2\text{O}_3$  (Alfa Aesar 99.9%) and  $\text{NaCl}$  (Merck 99.99%). The melt composition is 75.6 weight%  $\text{Bi}_2\text{O}_3$ , 17.9 weight%  $\text{Fe}_2\text{O}_3$ , and 6.5 weight%  $\text{NaCl}$ . Disregarding the  $\text{NaCl}$  that provides the sodium as a spectator ion, this translates to 56 mole%  $\text{Bi}_2\text{O}_3$  and 44 mole%  $\text{Fe}_2\text{O}_3$ . We regard the above material as the material with controlled impurities, finding that the mentioned 6.5 weight% consists of the optimal impurity composition for obtaining the highest BFO content after sintering. This was compared to results obtained with a composition of 78.85 weight%  $\text{Bi}_2\text{O}_3$  and 21.15 weight%  $\text{Fe}_2\text{O}_3$ , considered the material without controlled impurities. It gives ample room for study without the system shifting into a different phase system during the study due to mass loss. A recent article [13] illustrates this mass loss using DTA/TGA curves stating that above 400°C and up to 800°C approximately 2.5% Bi evaporation occurs. This corresponds to approximately a 1 mole% decrease in Bi content. Based on [3] we can assume that at 855°C it

increases to 7 mole% over a period of 24 hours. As shall be seen, the above compositions will assist us in evaluating dynamics and evolution of the different compounds in the sintered samples. The constituents were mixed and milled, followed by calcination at 800°C for 4 hours in alumina crucibles. The furnace was heated at a rate of 100 degrees per hour with the material inside until it reached the target temperature. After 4 hours of calcination it was cooled to room temperature at a rate of 100 degrees per hour. The calcinated material was ground for 2 hours using a ball grinder and sieved through a 50µm mesh. Approximately 0.6g was pressed uniaxially into 12.7 mm disks with a pressure of approximately 100MPa. Pressed disks were inserted into a muffle furnace set at 880°C for a certain period of time set in minutes and were extracted followed by quenching in air.

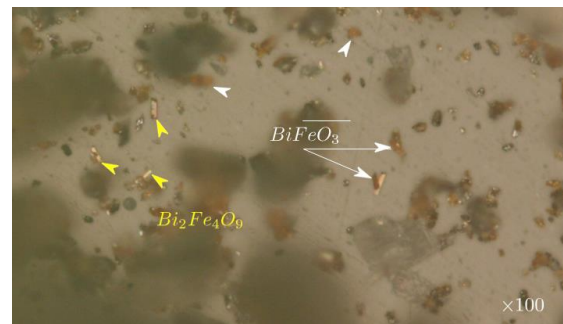


**Fig.1.** Fragments of crushed material after calcination prior to grinding. Much of the material has crystallized into its distinguishable phases

### Evaluation of the calcined materials

The resulting calcined materials and sintered samples were recorded visually using a metallurgical microscope, followed by XRD and SEM analysis. The XRD measurements were conducted on a Rigaku SmartLab using the SmartLab Studio II software for analysis. One of the most important aspects for comprehending the optical microscope images is the ability to distinguish the morphology of at least one of the phases. As we shall see from the XRD analysis, the three obtained crystalline phases important to us, are  $\text{BiFeO}_3$ ,  $\text{Bi}_2\text{Fe}_4\text{O}_9$  and  $\text{Bi}_{25}\text{FeO}_{40}$ . Based on the Gibbs energy of formation [14] during the initial stages of nucleation, and for a relatively short time a metastable  $\text{BiFeO}_3$  compound prevails over the  $\text{Bi}_2\text{Fe}_4\text{O}_9$  and the  $\text{Bi}_{25}\text{FeO}_{40}$ . It means as well, that the metastable compound will prevail at a lower temperature range. In the longer time span we expect the more stable compounds as are described by the  $\text{Bi}_2\text{O}_3$   $\text{Fe}_2\text{O}_3$  phase system. For

the 56/44 mole% Bi/Fe composition we expect either BFO or sillenite. We begin by analysing the compounds after calcination. Fig.1 illustrates an x100 optical microscope image of fragments of crushed calcinated material before grinding.

The figure illustrates that during the calcination process some of the constituents may be separated for analysis. In the example illustrated in the figure, two phases are distinguishable, the metallic color orthorhombic  $\text{Bi}_2\text{Fe}_4\text{O}_9$  and the orange tinted brown rhombohedral  $\text{BiFeO}_3$ . Crystal phases developed due to the calcination process were analysed by crushing some of the calcinated compounds rinsing them in  $\text{HNO}_3$  and washing them in water. This procedure dissolved all the different phases but the  $\text{Bi}_2\text{Fe}_4\text{O}_9$  and  $\text{BiFeO}_3$ . The two remaining crystals were manually separated and were analysed with XRD.

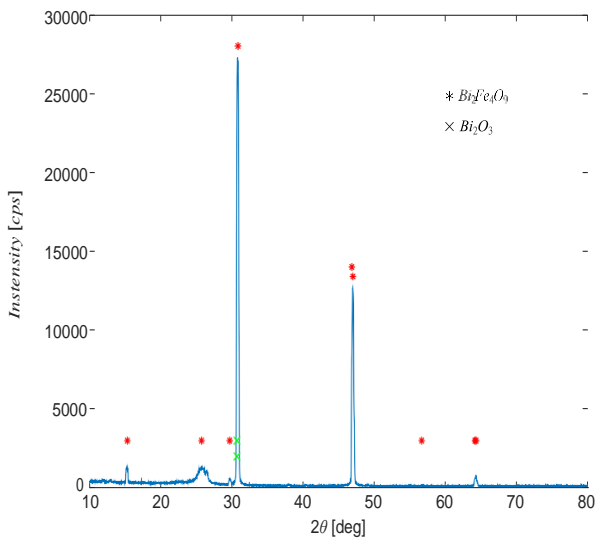
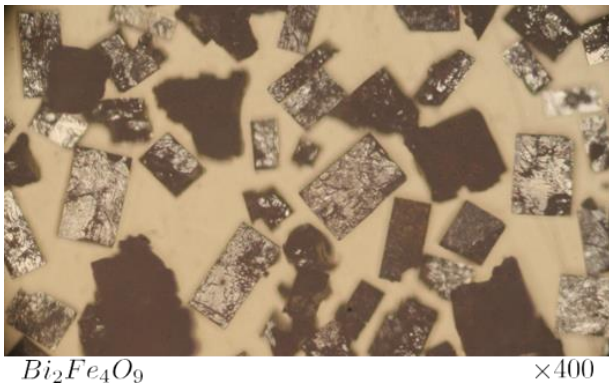


**Fig.2.**  $\text{Bi}_2\text{Fe}_4\text{O}_9$  crystals extracted from the calcinated material with its XRD profile

Fig.2 illustrates an example of separated  $\text{Bi}_2\text{Fe}_4\text{O}_9$  crystals.

For the above example using split pseudo-Voigt fitting of the diffraction peaks and fitting the peaks with the ICDD database. The lattice parameters were measured to be  $a = 7.9947\text{\AA}$ ;  $b = 8.4599\text{\AA}$ ;  $c = 5.9254\text{\AA}$ .

We now compare the crystallized compositions of the two synthesized materials (with  $\text{Bi}_2\text{O}_3$ ;  $\text{NaCl}$  flux and  $\text{Bi}_2\text{O}_3$  flux) after calcination and grinding. Fig.3 illustrates the ground material with 6.5 weight%  $\text{NaCl}$ .

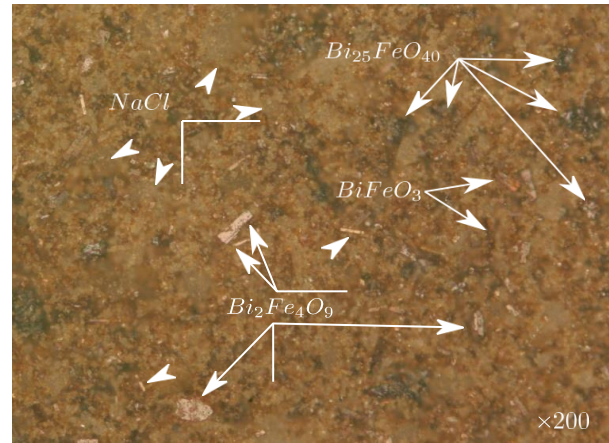


**Fig.3.** An optical microscope image of the synthesized and ground material with 6.5 weight%  $\text{NaCl}$  prior to sintering. An example of the various phases that can be observed is pointed using arrows

X-ray diffraction measurements of the ground material with  $\text{NaCl}$  in the flux show the following weight fraction of the crystalline phases (Tab.1).

**Table 1.** Weight fraction of crystalline phases in calcinated BFO  $\text{Bi}_2\text{O}_3$ ;  $\text{NaCl}$  based flux

Compound	Weight fraction [%]	a [Å]	b [Å]	c [Å]	$\alpha$ [°]	$\beta$ [°]	$\gamma$ [°]
$\text{Bi}_2\text{Fe}_4\text{O}_9$	27.4	7.96623	8.434444	5.99638	90.000	90.000	90.000
$\text{Bi}_{22}\text{Fe}_2\text{O}_{36}$	26.3	10.13167	10.13167	10.13167	90.000	90.000	90.000
$\text{Bi}_{25}\text{FeO}_{40}$	24.4	10.15868	10.15868	10.15868	90.000	90.000	90.000
$\text{BiFeO}_3$	14.6	5.63427	5.63427	13.78349	90.000	90.000	120.000
$\alpha\text{-BiFeO}_3$	7.3	5.62267	5.62936	5.62796	59.330	59.330	59.330

As we can expect, we see that the prevailing phases are the mullite (27.4%) and sillenite (24.4%). An additional, less commonly reported compound  $\text{Bi}_{22}\text{Fe}_2\text{O}_{36}$ , was observed as well. This compound was suggested by Mel'Nikova et al. [15] who developed a method of determining the composition of sillenites using XRD data. Murakami [16] working on  $\text{BaTiO}_3$   $\text{BiFeO}_3$  compounds, reports detecting the compound but does not dwell on the subject. We assume that it is one of the metastable phases which is attained due

to the existence of the sodium ions, acting as spectator ions. A smaller fraction (14.6%) of rhombohedral  $\text{BiFeO}_3$  phase exists with an additional 7.3% (2:1 ratio) of the triclinic (P1)  $\alpha$   $\text{BiFeO}_3$ . The  $\alpha$   $\text{BiFeO}_3$  results obtained, corresponds with the lattice parameters reported by Wang et al. [17]. It is interesting to notice that even though the NaCl did not react with the material displaying obvious segregation it was found to be in an amorphous state.

Fig.4 displays an optical microscope image of the second calcinated and ground  $\text{Bi}_2\text{O}_3$  based flux.

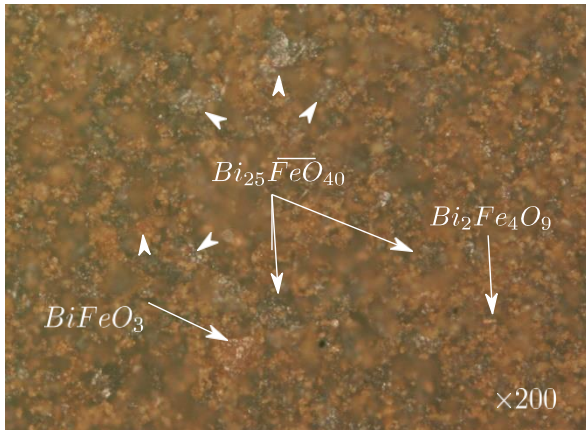


**Fig.4.** Optical microscope image of the calcinated and ground  $\text{Bi}_2\text{O}_3$  based flux

While the orthorhombic mullite structure is hardly observed in the figure, one can easily notice the considerable increase in the metallic grey areas signifying the sillenite compound. Tab.2 displays the weight fraction of the crystalline phases of the calcinated flux materials that do not include the sodium chloride.

**Table 2.** Weight fraction of crystalline phases in calcinated BFO flux materials without sodium chloride

Compound	Weight fraction [%]	a [Å]	b [Å]	c [Å]	$\alpha$ [°]	$\beta$ [°]	$\gamma$ [°]
$\text{Bi}_{25}\text{FeO}_{40}$	68.9	10.15600	10.15600	10.15600	90.000	90.000	90.000
$\text{BiFeO}_3$	25.7	5.57801	5.57801	13.86400	90.000	90.000	120.00
$\text{Bi}_2\text{Fe}_4\text{O}_9$	5.39	7.97971	8.43282	6.00463	90.000	90.000	90.000

Tab.2 shows a similar percentage of mullite to the material in which the parasitic phases were not reduced (Lu [3]). In this molar ratio we do expect the sillenite to be much more abundant as it is one of the two stable phases.

#### Sintering

Prior to sintering and in order to test the stable phases, the materials were placed for 16 hours at

600°C thus increasing the stable phases at that temperature range, i.e. - the mullite and sillenite phases. The reaction trend gives us a better indication which are the stable phases. As the various articles using rapid sintering [6, 7, 8] reported placing the pressed disks within the furnace between 400 and 450 seconds, the samples were placed in the furnace up to 8 minutes and then rapidly cooled by extracting them from the furnace and letting them cool on a piece of ceramic at room temperature. Fig.5 illustrates the results obtained from the 56/44 mole%  $\text{Bi}_2\text{O}_3/\text{Fe}_2\text{O}_3$  solid state compounds based on XRD measurements.

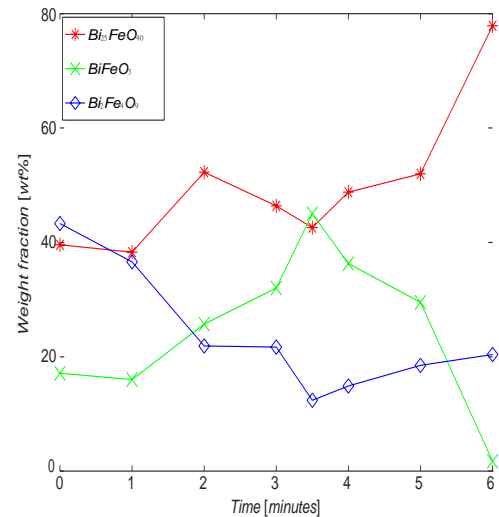


**Fig.5.** Weight fraction of the different compounds resulting from the solid-state reaction of the quenched disks at 880°C based on the reaction time

At this specific  $\text{Bi}_2\text{O}_3/\text{Fe}_2\text{O}_3$  ratio, the two expected phases that are known to coexist are the BFO phase and the sillenite phase. The results show that up to approximately 3.5 minutes the  $\text{BiFeO}_3$  phase increased to about 50% at the expense of both the  $\text{Bi}_{25}\text{FeO}_{40}$  and  $\text{Bi}_2\text{Fe}_4\text{O}_9$  phases, after which it experiences a fast decline to undetectable levels. After 3.5 minutes while the BFO decomposes the level of the mullite increases slightly and the sillenite becomes the dominant stable phase. This does not correspond with the accepted phase diagram and hints that some impurities from the crucible may have altered the composition or that at 880°C  $\text{Bi}_{25}\text{FeO}_{40}$  is the dominant phase.

We repeated the process described above, with the  $\text{Bi}_2\text{O}_3/\text{Fe}_2\text{O}_3/\text{NaCl}$  composition. The weight fraction of the different compounds obtained by the system as a function of time is described in Fig.6.

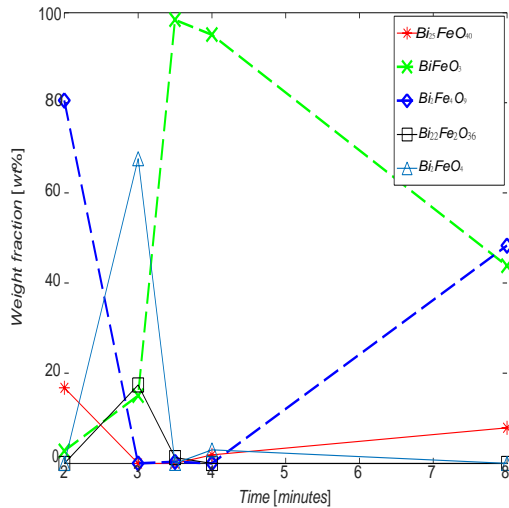


**Fig. 6.** Weight fraction of the different compounds obtained by the  $56\text{Bi}_2\text{O}_3 \cdot 44\text{Fe}_2\text{O}_3 + 6.5\text{wt}\% \text{NaCl}$  composition heated and quenched disks at  $880^\circ\text{C}$  based on the reaction time.

Fig. 6 demonstrates the process in which the NaCl (Melting point  $801^\circ\text{C}$ ) slowly, dissolves the constituents and between 3-4 minutes suppressing the mullite and sillenite phases while the BiFeO<sub>3</sub> temporarily dominates. At this composition, the material is beyond the peritectic which for longer periods will result in a liquid + Bi<sub>2</sub>Fe<sub>4</sub>O<sub>9</sub> similar to the transition, for the 56/44 mole% composition above  $934^\circ\text{C}$ .

## DISCUSSION

Based on the accepted phase diagram [18, 9, 10, 11, 3], and Gibbs energy of formation [14], during the synthesis of materials and solid state reactions above  $767^\circ\text{C}$  the Bi<sub>2</sub>Fe<sub>4</sub>O<sub>9</sub> phase, should not be a stable phase. This is true as long as the Bi<sub>2</sub>O<sub>3</sub>/Fe<sub>2</sub>O<sub>3</sub> molar ratio is above 1:2. Contrary to what has just been stated, experience has shown that for long enough periods of time the mullite phase does form as a stable phase. As a result, rapid heating and cooling techniques are a common practice for obtaining a high weight fraction of BFO ceramics. Lu et. al. have shown that for highly controlled compositions in gold crucibles at a temperature of  $850^\circ\text{C}$ , BFO is the prevalent stable phase. Given impurities it will slowly decompose to other phases primarily to mullite. At temperatures above  $855^\circ\text{C}$  even the highly controlled compositions tend to decompose over a long period of time. This has to be taken into account if one attempts to grow bulk crystals even for highly controlled environments, one is limited below  $850^\circ\text{C}$  for bulk BFO crystal growth. As the goal of this work was sintering

targets for sputtering machines, we were interested in BFO phase stability and the adequate sintering time during the sintering process. We compared a 56:44 mole% Bi<sub>2</sub>O<sub>3</sub>-Fe<sub>2</sub>O<sub>3</sub> composition to a  $56\text{Bi}_2\text{O}_3 \cdot 44\text{Fe}_2\text{O}_3 + 6.5\text{wt}\% \text{NaCl}$  composition. We demonstrated that at  $880^\circ\text{C}$  after 3.5 minutes in the composition which does not include NaCl only approximately 50% of the material has transformed into BFO. At the same time using the composition that includes NaCl as a flux, 98.5% of the material was in the BFO phase totally suppressing any other phase. Further work is being carried out in order to increase the BFO content for at least 99.98% obtaining the required grade for RF sputtering purposes. The importance of this finding is that it is relatively simple to remove the NaCl from the sintered disk. This is done by rinsing the disk in water. One drawback of this method is that it leaves the disk with pitting and cavities.

## CONCLUSIONS

In this article a simple method for rapid sintering of BFO targets for RF sputtering purposes is demonstrated. The targets are significant for applications in photovoltaic, memory and sensor design based on BFO, mullite or a combination of both phases as discussed in [19]. A 56/44 Bi<sub>2</sub>O<sub>3</sub>/Fe<sub>2</sub>O<sub>3</sub> + 6.5wt% NaCl composition was shown to give superior results in rapid sintering of targets compared to the same composition without the NaCl. It is important to note that the NaCl did not form new phases or compounds but provides the sodium as a spectator ion. After the sintering process, the NaCl was extracted from the target by rinsing in water. We note that the suggested experimental setting is providing a good preliminary BFO composition. However, the concentration should be further increased in order to employ it as a BFO sputtering target.

## REFERENCES

- [1] Nicola A Spaldin, Sang-Wook Cheong, and Ramamoorthy Ramesh. Multiferroics: Past, present, and future. *Physics Today*, **63**(10), 38 (2010).
- [2] Gustau Catalan, James F Scott. Physics and applications of bismuth ferrite. *Advanced materials*, **21**(24), 2463–2485 (2009).
- [3] J Lu, LJ Qiao, PZ Fu, YC Wu. Phase equilibrium of Bi<sub>2</sub>O<sub>3</sub>-Fe<sub>2</sub>O<sub>3</sub> pseudo-binary system and growth of BiFeO<sub>3</sub> single crystal. *Journal of crystal growth*, **318**(1), 936–941 (2011).
- [4] S Phapale, R Mishra, D Das. Standard enthalpy of formation and heat capacity of compounds in the

- pseudo-binary Bi<sub>2</sub>O<sub>3</sub>–Fe<sub>2</sub>O<sub>3</sub> system. *Journal of nuclear materials*, 373(1- 3), 137–141 (2008).
- [5] TT Carvalho and PB Tavares. Synthesis and thermodynamic stability of multiferroic BiFeO<sub>3</sub>. *Materials Letters*, 62(24), 3984–3986 (2008).
- [6] JAHAR L MUKHERJEE, FRANKLIN FY WANG. Kinetics of solid-state reaction of Bi<sub>2</sub>O<sub>3</sub> and Fe<sub>2</sub>O<sub>3</sub>. *Journal of the American Ceramic Society*, 54(1), 31–34 (1971).
- [7] YP Wang, L Zhou, MF Zhang, XY Chen, J-M Liu, and ZG Liu. Room-temperature saturated ferroelectric polarization in BiFeO<sub>3</sub> ceramics synthesized by rapid liquid phase sintering. *Applied Physics Letters*, 84(10), 1731–1733 (2004).
- [8] MS Awan and AS Bhatti. Synthesis and multiferroic properties of BFO ceramics by melt-phase sintering. *Journal of materials engineering and performance*, 20(2), 283–288 (2011).
- [9] EI Speranskaya, VM Skorikov, E Ya Rode, VA Terekhova. The phase diagram of the system bismuth oxide–ferric oxide. *Bulletin of the Academy of Sciences of the USSR, Division of chemical science*, 14(5), 873–874 (1965).
- [10] A Maitre, M Francois, and JC Gachon. Experimental study of the Bi<sub>2</sub>O<sub>3</sub>-Fe<sub>2</sub>O<sub>3</sub> pseudo-binary system. *Journal of Phase Equilibria and Diffusion*, 25(1), 59–67 (2004).
- [11] R Palai, RS Katiyar, Hans Schmid, Paul Tissot, SJ Clark, Jv Robertson, SAT Redfern, GA Catalan, JF Scott.  $\beta$  phase and  $\gamma$ -  $\beta$  metal-insulator transition in multiferroic BiFeO<sub>3</sub>. *Physical Review B*, 77(1), 014110 (2008).
- [12] ZV Gabbasova, MD Kuzm' in, AK Zvezdin, IS Dubenko, VA Murashov, DN Rakov, IB Krynetsky. Bi(1-x)R(x)FeO<sub>3</sub>(R= rare earth): a family of novel magnetoelectrics. *Physics Letters A*, 158(9), 491-498 (1991).
- [13] Piyush Sharma, PK Diwan, OP Pandey. Impact of environment on the kinetics involved in the solid-state synthesis of bismuth ferrite. *Materials Chemistry and Physics*, 233, 171–179 (2019).
- [14] Sverre M Selbach, Mari-Ann Einarsrud, Tor Grande. On the thermodynamic stability of BiFeO<sub>3</sub>. *Chemistry of Materials*, 21(1), 169–173 (2009).
- [15] TI Mel'nikova, GM Kuz'micheva, NB Bolotina, NV Sadovskaya. Development of methods of X-ray diffraction analysis for determining the composition and structure of sillenite-family crystals. *Crystallography Reports*, 59(2), 155–159 (2014).
- [16] Shunsuke Murakami. BaTiO<sub>3</sub>-BiFeO<sub>3</sub> based lead-free ceramics for actuator applications. PhD thesis, University of Sheffield, 2018.
- [17] Hui Wang, Chengxu Yang, Jun Lu, Meimei Wu, Jie Su, Kuo Li, Junrong Zhang, Guobao Li, Tounan Jin, Takashi Kamiyama, et al. On the structure of  $\alpha$ -BiFeO<sub>3</sub>. *Inorganic chemistry*, 52(5), 2388–2392 (2013).
- [18] Hideo Koizumi, Nobukazu Niizeki, and Takuro Ikeda. An X-ray study on Bi<sub>2</sub>O<sub>3</sub>-Fe<sub>2</sub>O<sub>3</sub> system. *Japanese Journal of Applied Physics*, 3(8), 495–496 (1964).
- [19] A.S. Poghossian, H.V. Abovian, P.B. Avakian, S.H. Mkrtchian, V.M. Haroutunia. Bismuth ferrites: New materials for semiconductor gas sensors. *Sensors and Actuators B: Chemical*, 4(3), 545-549 (1991).